The American Journal of Pathology, Vol. 187, No. 3, March 2017

The American Journal of
PATHOLOGY
ajp.amjpathol.org

ANIMAL MODELS

HANAC *Col4a1* Mutation in Mice Leads to Skeletal Muscle Alterations due to a Primary Vascular Defect

Simon Guiraud,[*†‡] Tiffany Migeon,[*†] Arnaud Ferry,[§] Zhiyong Chen,[*] Souhila Ouchelouche,[*†] Marie-Christine Verpont,[*†] Yoshikazu Sado,[¶] Valérie Allamand,[§] Pierre Ronco,[*†‖] and Emmanuelle Plaisier[*†‖]

From the Mixed Research Unit S1155, INSERM, Paris, France; the University Pierre and Marie Curie Paris 06,[†] the Sorbonne University, Paris, France; the Medical Research Council Functional Genomics Unit,[‡] Department of Physiology, Anatomy, and Genetics, University of Oxford, Oxford, United Kingdom; the Research Center in Myology,[§] Institut de Myologie, the Inserm UMRS974, CNRS FRE3617, Pitié-Salpêtrière Hospital Group, University Pierre and Marie Curie Paris 06, Paris Descartes University, The Sorbonne University, Paris, France; the Shigei Medical Research Institute,[¶] Okayama, Japan; and the Department of Nephrology and Dialysis,[‖] Assistance Publique-Hôpitaux de Paris, Tenon Hospital, Paris, France*

Accepted for publication October 25, 2016.

Address correspondence to Emmanuelle Plaisier, M.D., Ph.D., INSERM UMR_S 1155, Hôpital Tenon, 4 Rue de la Chine, 75020 Paris, France. E-mail: emmanuelle.plaisier@tnn.aphp.fr.

Collagen IV is a major component of basement membranes (BMs). The α1(IV) chain, encoded by the *COL4A1* gene, is expressed ubiquitously and associates with the α2(IV) chain to form the α1α1α2(IV) heterotrimer. Several *COL4A1* mutations affecting a conformational domain containing integrin-binding sites are responsible for the systemic syndrome of hereditary angiopathy, nephropathy, aneurysms, and cramps (HANAC). To analyze the pathophysiology of HANAC, *Col4a1* mutant mice bearing the p.Gly498Val mutation were generated. Analysis of the skeletal muscles of $Col4a1^{G498V}$ mutant animals showed morphologic characteristics of a muscular dystrophy phenotype with myofiber atrophy, centronucleation, focal inflammatory infiltrates, and fibrosis. Abnormal ultrastructural aspects of muscle BMs was associated with reduced extracellular secretion of the mutant α1α1α2(IV) trimer. In addition to muscular dystrophic features, endothelial cell defects of the muscle capillaries were observed, with intracytoplasmic accumulation of the mutant α1α1α2(IV) molecules, endoplasmic reticulum cisternae dilation, and up-regulation of endoplasmic reticulum stress markers. Induction of the unfolded protein response in *Col4a1* mutant muscle tissue resulted in an excess of apoptosis in endothelial cells. HANAC mutant animals also presented with a muscular functional impairment and increased serum creatine kinase levels reflecting altered muscle fiber sarcolemma. This extensive description of the muscular phenotype of the *Col4a1* HANAC murine model suggests a potential contribution of primary endothelial cell defects, together with muscle BM alterations, to the development of *COL4A1*-related myopathy. *(Am J Pathol 2017, 187: 505–516; http://dx.doi.org/10.1016/j.ajpath.2016.10.020)*

The basement membrane (BM) is a specialized extracellular matrix (ECM) that is present in nearly all organs, including vessels, muscle, kidney, skin, central and peripheral nervous systems, eye, and adipose tissue. In addition to their structural role, BMs are involved in cell differentiation, migration, and proliferation.[1] The main molecular components of BMs include collagen IV, laminin heterotrimers, heparin sulfate proteoglycans, and entactin/nidogen. In muscle BMs, the collagen IV network is composed of the ubiquitously expressed α1 and α2(IV) chains that assemble to form the α1α1α2 heterotrimer.[2]

Supported by the Université Pierre et Marie Curie Paris 6-Emergence grant EME1120 (E.P., S.G., V.A.), the National Research Agency grant ANR-08 Genopath-018 (P.R., E.P.), the European Community-7th Framework Program (European Network for the Study of Orphan Nephropathies) grant HEALTH-F2-2007-201590 (P.R., E.P.), The Association Française contre les Myopathies AFM-Téléthon grant 18712, the Association pour l'Information et la Recherche sur les maladies Rénales Génétiques (E.P.), and the Foundation Lefoulon-Delalande-Institut de France (S.G.).

Disclosures: E.P. and P.R. have received financial support from Amgen Inc.

http://dx.doi.org/10.1016/j.ajpath.2016.10.020

Several congenital muscular dystrophies arise from mutations in genes encoding for either muscular ECM proteins, including collagen VI and laminin α2, or cell surface receptors that interact with BM proteins, especially integrin α7 and the dystroglycan complex.[3–6] These observations underline the crucial role of the ECM and the fiber cytoskeleton in the structural and functional integrity of skeletal muscle.

Mutations of the *COL4A1* gene, encoding the α1 chain of type IV collagen, were reported first in patients presenting with autosomal-dominant cerebral small-vessel disease, which is responsible for stroke, porencephaly, leukoencephalopathy, and neurologic symptoms, sometimes associated with eye defects.[7–11] An asymptomatic increase of serum creatine kinase (CK) levels was reported in 6 of 15 patients presenting with cerebral small-vessel disease related to *COL4A1* pathogenic variants, and one patient showed histologic signs of myopathy that associated endomysial fibrosis and centronucleation.[12]

We characterized a distinct phenotypic presentation within *COL4A1*-related diseases: hereditary angiopathy, nephropathy, aneurysms, and cramps (HANAC).[13–15] HANAC patients present with systemic symptoms that usually associate a cerebral small-vessel disease of mild severity, retinal arteriolar tortuosity, renal defects, and a muscle disease. Common muscular signs include cramps appearing during early childhood, slight defects in muscle strength in adult women, and a persistent increase of CK levels. *COL4A1* missense mutations responsible for HANAC all closely localize in exons 24 and 25 and substitute glycine residues between Gly498 and Gly528 residues, within the cyanogen bromide–derived fragment CB3(IV) of the α1α1α2(IV) collagenous domain that contains α1β1, α2β1, and α3β1 integrin-binding sites.[15–18] Because *COL4A1* mutations associated with the brain-restricted phenotype usually are localized in the C-terminal half of the protein, these data suggested a phenotype–genotype correlation within *COL4A1*-related diseases.

Several *Col4a1* N-ethyl N-nitrosourea mutant mice are available, but they all bear mutations that do not affect the Gly498–Gly528 region.[7,19,20] To analyze the pathogenesis of HANAC specifically, we generated a mutant mouse strain bearing the *Col4a1* p.Gly498Val substitution that is homologous to the human *COL4A1* HANAC pGly498Val mutation. We previously showed the relevance of this murine strain for the analysis of HANAC renal defects.[21] In the present study, we describe the muscular phenotype of *Col4a1* HANAC mutant animals.

Materials and Methods

Animals

The *Col4a1 G498V* mouse line was established by homologous recombination, as previously described.[21] Mice were maintained in a specific pathogen-free environment and experiments were conducted in accordance with French government policies (Services Vétérinaires de la Santé et de la Production Animale, Ministère de l'Agriculture, agreement number B752001; Ministère de l'Education Nationale, de l'Enseignement Supérieur et de la Recherche, agreement number 01108.03).

Histology and Morphometrics

Six-month-old mice were sacrificed via cervical dislocation. Tibialis anterior (TA), extensor digitorum longus, quadriceps (QUAD), gastrocnemius, soleus, and triceps (TRI) muscles were frozen in liquid nitrogen–chilled isopentane, and stored at −80°C. The single-fiber area and fiber number were determined as follows: cryosections (8-μm thick) were treated for 20 minutes with H_2O_2, blocked with 10% goat serum in phosphate-buffered saline, incubated with rabbit antilaminin antibody (1:400, 10765; Progen, Heidelberg, Germany) for 2 hours at room temperature, followed by goat anti-rabbit horseradish peroxidase–labeled antibody (1:200, P0448; Dako, Courtaboeuf, France). Sections were mounted with Eukitt (Labonord, Villeneuve, D'ASCQ, France) after treatment with di-amino-3,30 benzidine. Digital images were captured using a charge coupled device camera (Sony, FAS Film, Evry, France) and processed using Ellix software version 7.7 (Microvision, Evry, France). Cryosections (8-μm thick) were stained with hematoxylin and eosin solution, Sirius red, and Masson trichrome, and analyzed using the Axioplan 2 Microscope System (Carl Zeiss, Göttingen, Germany). For fibrosis quantification, cross-sections on the larger diameter of the right and left TA, TRI, and QUAD (one cross-section/muscle, 3 animals/group) were incubated with 1% Sirius red F3B (BDH Chemicals, VWR International SAS, Fontenay sous Bois, France) in Bouin Duboscq Brasil Liquid (526271; Carlo ERBA Reagents, Val de Reuil, France). Fibrosis was quantified using morphometric analysis software (AnalySIS version 5.0 Build 1131; Soft Imaging System Gmbh, Münster, Germany) that allowed the formation of a binary image in which the stained area was calculated as a percentage of the image area. Data were expressed as the mean value of the percentage of the positive area analyzed. The percentage of embryonic myosin heavy chain (eMHC)-positive fibers was determined on whole transverse sections of TRI muscle, stained with anti-eMHC antibodies (3 sections/muscle and 3 animals/genotype), with positive eMHC fibers counted by manual tag using ImageJ version 1.6.0 (NIH, Bethesda, MD; *http://imagej.nih.gov/ij*) and divided by the number of total fibers in the section maps. Total fiber counts ranged from 1687 to 3209.

Immunofluorescence

Frozen muscle sections (8-μm thick) were blocked in 10% fetal bovine serum in phosphate-buffered saline for 30 minutes, incubated with primary antibodies overnight at 4°C,

washed in phosphate-buffered saline, and incubated with suitable Alexa Fluor secondary antibodies for 2 hours at room temperature. Sections were examined under a confocal microscope (TCS-SP2; Leica, Wetzlar, Germany). The following primary antibodies were used: rat anti-α1(IV) chain (1:50, H11, a gift from Y. Sato), rat anti-α2(IV) chain (1:50, H22; a gift from Y. Sato), rabbit anti−collagen IV (1:800, 20451; Novotec, Lyon, France), rabbit anti−collagen I (1:100, 600-401-103-01; Rockland, TEBU Bio, Le Perray en Yveline, France), rabbit anti−collagen VI (1:100, ab6588; Abcam, Paris, France), rabbit anti-fibronectin (1:200, ab2413; Abcam), rat antiperlecan (1:50, 05-209; Millipore, Billerica, MA), rabbit anti−binding immunoglobulin protein/78 kDa glucose regulated protein (BiP/GRP78; 1:50, ab21685; Abcam), mouse anti−heat shock protein 47 (1:50, SPA-470; Stressgen, Enzo Life, Villeurbane, France), mouse anti−protein disulfide isomerase (1:50, SPA-891; Stressgen), goat anti−platelet endothelial cell adhesion molecule 1/CD31 (1:50, SC-1506; Santa Cruz, Cliniscience, Nanterre, France), monoclonal rat anti-β1 subunit of very late antigen β1 integrins (1:50, MAB1997; Millipore), mouse monoclonal anti-embryonic myosin heavy chain (1:20, F1.652; Developmental Studies Hybridoma Bank, Iowa City, IO), rabbit antidystrophin (1:100, ab15277; Abcam), and rabbit peroxidase-conjugate anti-mouse IgG (1:100, 6170-02; Southern Biotech, Cliniscience, Nanterre, France).

Electron Microscopy

Ultrastructural analysis was performed on muscle samples fixed in 2.5% glutaraldehyde in 0.1 mmol/L cacodylate buffer (pH 7.4) at 4°C for 24 hours. Fragments were fixed afterward in 1% osmium tetroxide, dehydrated, and embedded in epoxy resin. Ultrathin sections (60 nm) were contrast-enhanced using uranyl acetate and lead citrate, and examined using a JEOL 1010 electron microscope (JEOL, Ltd., Tokyo, Japan) with a MegaView III camera (Olympus Soft Imaging Systems GmbH, Münster, Germany).

Western Blot

Frozen muscle was ground and homogenized in a RIPA Lysis Buffer System (SC-24948; Santa Cruz). Sixty micrograms of total protein was heat-denatured, separated by SDS-PAGE, and transferred to a polyvinylidenedifluoride membrane (Bio-Rad, Marne La Coquette, France). After blocking, membranes were incubated overnight at 4°C with primary antibodies and subsequently suitable horseradish peroxidase−conjugated secondary antibodies. Immunoreactive bands were detected using ECL Western Blot detection reagents (SuperSignal West Pico Chemiluminescent Substrate; Thermo Scientific, Saint Aubain, France). The relative expression of the target proteins was estimated by densitometry using glyceraldehyde-3-phosphate dehydrogenase as reference on a CHEMI SMART 5000 system (Vilbert Lourmat, Marne la Vallée, France) and Chemi-Capt 2000 version 12.6a software (Vilbert Lourmat). The following primary antibodies were used: rabbit anti-GRP78/BiP (1:1000, 21685; Abcam), rabbit anti−protein disulfide isomerase (1:500, ab31811; Abcam), rabbit anticalnexin (1:500, ab10286; Abcam), rabbit anti−C/EBP homologous protein (1:1000, 5554; Cell Signaling, Cliniscience, Nanterre, France), and rabbit anti−glyceraldehyde-3-phosphate dehydrogenase (1:10,000, G9545; Sigma-Aldrich, Saint Quentin Fallavier, France). Secondary antibodies included horseradish peroxidase−conjugated goat anti-rabbit Ig (1:4000, ab97051; Abcam) and horseradish peroxidase−conjugated rabbit anti-goat Ig antibodies (1:5000, 81-1620; Invitrogen, Illkrich, France).

RNA Extraction and Quantitative PCR Analysis

QUAD muscles from 6-month-old animals were homogenized using a hand-held homogenizer (IKA S10N-5G; IKA, Staufen, Germany) before extraction of RNA using TRI Reagent (Euromedex, Mundolsheim, France). RNA concentration was determined using a Nanodrop 300 spectrophotometer (Labtech, Palaiseau, France). After digestion with DNase I, total RNA was reverse-transcribed using the RevertAid First Strand cDNA Synthesis Kit (Thermo Scientific). Primers for X-box−binding protein 1 unspliced (primer sequences: forward: 5′-TGCTGAGTCCGCAGCAGGTG-3′, reverse 5′-TGCTGAGTCCGCAGCA-3′) and X-box−binding protein 1 spliced (primer sequences: forward 5′-CTGACGAGGTTCCAGAGGTG-3′, reverse 5′-GCAGAGGTGCACATAGTCTGAG-3′) mRNAs were designed using the Universal Probe Library (Roche Diagnostics, Meylan, France) website. The cDNA was amplified by PCR in a LightCycler 480 (Roche Diagnostics) with SYBR Green (Fast Start DNA Master SYBR Green I; Roche Diagnostics) under the following conditions: 95°C for 5 minutes, 45 cycles at 95°C for 15 seconds and 60°C for 15 seconds, and 72°C for 15 seconds. Quantitative PCR also was performed for the housekeeping gene, β-glucuronidase (primer sequences: forward 5′-CTCTGGTGGCCTTACCTGAT-3′, reverse 5′-CAGTTGTTGTCACCTTCACCTC-3′). Results are expressed as $2^{-\Delta CT}$, where C_T is the cycle threshold number normalized to the mean $2^{-\Delta CT}$ for each corresponding control group. Dissociation curves were analyzed after each run for each amplicon to determine the specificity of quantification when using SYBR Green.

Apoptosis Study

A terminal deoxynucleotidyl transferase-mediated dUTP nick-end labeling assay was performed on 8-μm TRI muscle cryosections (3 sections/muscle and 3 animals/genotype) using the ApopTag plus peroxidase *in situ* apoptosis detection kit (cat. S7101; Millipore) according to the manufacturer's instructions. The sections were incubated with deoxynucleotidyl transferase, developed with the diaminobenzidine detection system, and then were counterstained

with methyl green (Vector Laboratories, Cliniscience, Nanterre, France). Whole transverse muscle images were captured at ×40 magnification and terminal deoxynucleotidyl transferase-mediated dUTP nick-end labeling–positive nuclei were counted by manual tag using ImageJ software for quantification.

Caspase-3 and caspase-12 activities were determined in duplicate in muscle protein extracts using the caspase-3/CPP32 Colorimetric Assay Kit (K106-25; Biovision, Milpitas, CA) and the caspase-12 Fluorometric Assay Kit (K139-25; Biovision), respectively. The caspase-3 assay was based on the spectrophotometric detection of the chromophore p-nitroanilide after cleavage from the labeled substrate N-acetyl-Asp-Glu-Val-Asp–p-nitroanilide. The caspase-12 assay was based on the detection of cleavage of substrate N-acetyl-Ala-Thr-Ala-Asp–7-amino-4-trifluoromethyl coumarin. The p-nitroanilide light emission and cleavage of substrate N-acetyl-Ala-Thr-Ala-Asp–7-amino-4-trifluoromethyl coumarin were quantified using the FLX-Xenius Spectrophotometers (SAFAS, Monaco, Monaco) at an OD of 405 nm (caspase-3) and 400-nm excitation filter and 505-nm emission filter (caspase-12).

Force Measurements

Muscle force measurements were evaluated by measuring *in situ* muscle contraction in response to nerve and muscle stimulation, as described previously.[22] Mice were anesthetized using a pentobarbital solution (60 mg/kg intraperitoneally). The distal tendon of the TA was detached and tied with a silk ligature to an isometric transducer (Harvard Bioscience, Holliston, MA). The sciatic nerve was stimulated distally, and the response to tetanic stimulation (pulse frequency, 50 to 143 Hz) was recorded and absolute maximal force was determined. The specific maximal force was calculated by dividing the absolute maximal force by the muscle weight measured just after the force test.

Serum CK Measurement

Retro-orbital blood was collected in 3-month-old animals that were anesthetized fully using inhaled isoflurane. Blood was centrifuged at 9500 × *g* for 10 minutes at 4°C. The serum CK level was determined using the Creatine Kinase Activity Assay Kit (MAK116; Sigma Aldrich), according to the manufacturer's instructions.

Statistics

Statistical significance was determined using either nonparametric tests (including the Mann–Whitney and Kruskal–Wallis tests, χ^2 test), or the paired *t*-test, when appropriate. Statistical significance was defined by a P value less than 0.05, 0.01, and 0.001. SD was used for all quantification.

Results

Col4a1–G498V Mutant Mice Suffer from Muscular Dystrophy

Cross-breeding of $Col4a1^{+/G498V}$ mice generated 32% of $Col4a1^{+/+}$, 51% of $Col4a1^{+/G498V}$, and 17% of $Col4a1^{G498V/G498V}$, with a significant increase of embryonic lethality of the $Col4a1^{G498V/G498V}$ female (Supplemental Table S1). However, heterozygous and homozygous $Col4a1^{G495V}$ mice of both sexes showed normal viability and fertility after birth.

Table 1 Body and Muscle Weights of 6-Month-Old Wild-Type and *Col4a1* HANAC Mutant Mice

Parameter	$Col4a1^{+/+}$ $n = 4$	$Col4a1^{+/G498V}$ $n = 4$	$Col4a1^{G498V/G498V}$ $n = 4$
Females			
Body weight, g	25.69 ± 4.28	23.78 ± 1.88	21.10 ± 2.40
Muscle weight, mg	$n = 8$	$n = 8$	$n = 8$
Extensor digitorum longus	8.89 ± 1.58	7.43 ± 0.55*	6.06 ± 0.56**†
Soleus	10.46 ± 0.89	5.55 ± 0.56**	5.20 ± 0.81**
Tibialis anterior	45.25 ± 4.52	43.64 ± 2.11	36.24 ± 3.93**†
Quadriceps	186.04 ± 11.91	168.94 ± 4.93***	154.54 ± 17.31***
Triceps	96.78 ± 7.53	83.49 ± 3.92**	84.41 ± 6.05***
Males			
Body weight, g	35.63 ± 6.84	30.33 ± 3.21	27.08 ± 2.51
Muscle weight, mg	$n = 8$	$n = 8$	$n = 8$
Extensor digitorum longus	10.33 ± 1.29	8.62 ± 1.51*	7.70 ± 0.46**
Soleus	8.94 ± 1.03	8.55 ± 0.60	8.13 ± 0.98
Tibialis anterior	57.59 ± 3.32	50.79 ± 1.37**	44.53 ± 2.07**††
Quadriceps	218.86 ± 12.41	193.14 ± 11.37***	181.23 ± 17.41**
Triceps	120.99 ± 6.30	106.73 ± 16.41*	91.87 ± 5.40**

Data are presented as means ± SD.
*$P < 0.05$, **$P < 0.001$, and ***$P < 0.01$ ($Col4a1^{+/G498V}$ and $Col4a1^{G498V/G498V}$ versus $Col4a1^{+/+}$).
$^{\dagger}P < 0.001$, $^{\dagger\dagger}P < 0.05$ ($Col4a1^{G498V/G498V}$ versus $Col4a1^{+/G498V}$).

At 6 months of age, *Col4a1* mutant animals had a reduced total body weight compared with $Col4a1^{+/+}$ mice, although statistical difference was not reached (Table 1). Muscle weight showed a significant decrease in $Col4a1^{G498V/G498V}$ animals, affecting the TA, extensor digitorum longus, QUAD, soleus, and TRI muscles. Muscle weight was affected less severely in heterozygous mutants, although it also was decreased significantly for several muscles (Table 1). Similar data were recorded in males (Table 1). The single-fiber area, evaluated in TA and TRI muscles of female mice, showed fiber atrophy in heterozygous and homozygous animals, with a mean single-fiber area reduction of 21.7% ($P = 0.03$) and 35.2% ($P = 0.0015$) in TA, and of 15.6% ($P = 0.03$) and 21.5% ($P = 0.009$) in TRI, respectively (Figure 1, A and B). The mean number of fibers in TA and TRI, however, was similar in all genotypes (Figure 1C), indicating that the reduced muscle mass in HANAC mutant mice was related to fiber atrophy but not to fiber hypoplasia, with a greater severity in homozygous mutants.

Histologic analyses of muscles disclosed several characteristics of muscular dystrophy (Figure 1D). The number of myofibers with nonperipheral nuclei was increased in heterozygous and homozygous *Col4a1* mutant muscles, by 117% and 328% in TA, and by 132% and 619% in TRI, respectively (Figure 1, D and E). In addition, staining with embryonic myosin heavy chain, transiently expressed in nascent myofibers at the initial phase of regeneration, showed a significantly higher proportion of positive myofibers in Col4a1 homozygous mutant TRI muscles, representing less than 1% of the total fibers, as compared with wild-type and heterozygous animals (Supplemental Figure S1). Both results indicated an abnormal induction of muscle regeneration in *Col4a1* HANAC mutant mice. Sirius red staining showed fibrillar collagens accumulation in endomysium of mutant muscles (Figure 1D) and fibrosis quantification in TA, TRI, and QUAD muscles showed an 8% to 63% increase of Sirius red–positive surface in heterozygous mice, and a 21% to 99% increase in $Col4a1^{G498V/G498V}$ mice compared with controls

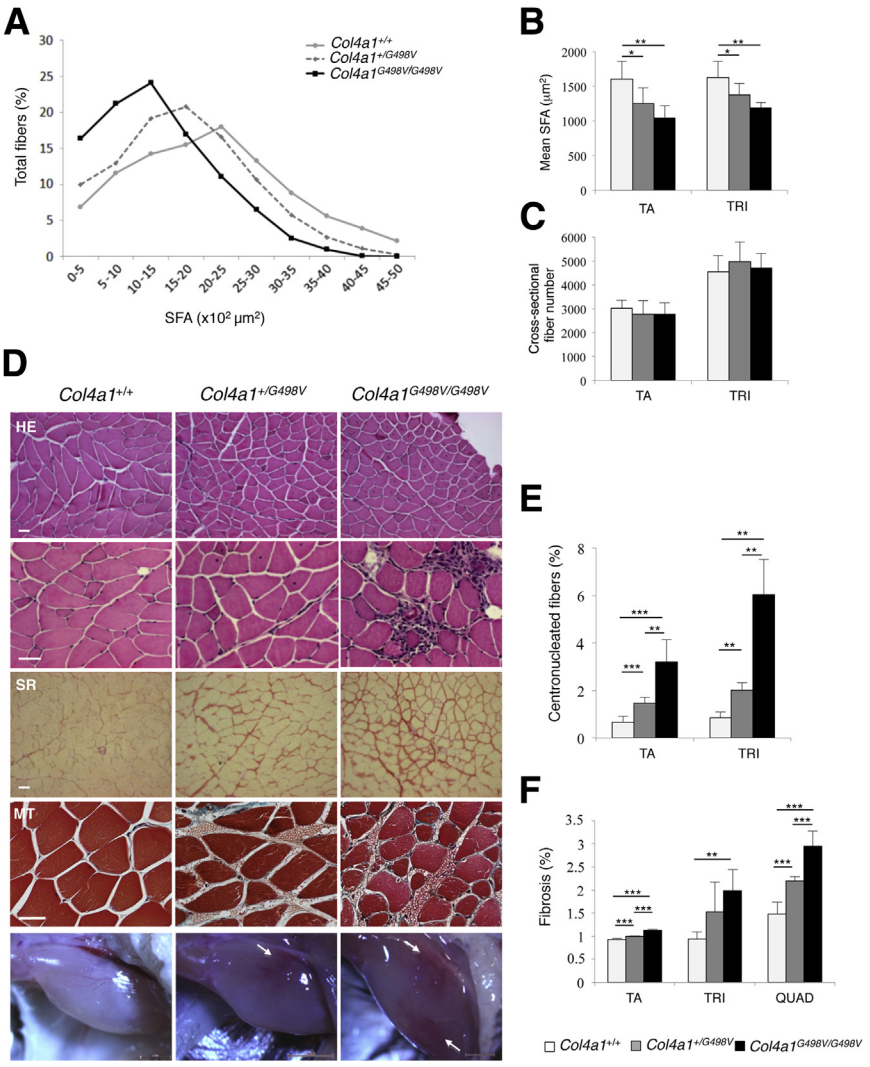

Figure 1 Morphologic characteristics of *Col4a1* HANAC muscles. **A:** Distribution of single-fiber area (SFA) in tibialis anterior muscle (TA) showed a shift to smaller SFA range in $Col4a1^{+/G498V}$ and $Col4a1^{G498V/G498V}$ compared with $Col4a1^{+/+}$ animals (3000 myofibers analyzed per TA muscle and data collected from 4 animals per group). **B:** Quantification of the SFA in TA and triceps (TRI) showed fiber atrophy in both heterozygous and homozygous HANAC mutant mice (4 animals/group and per muscle). **C:** Cross-sectional fiber numbers in TA and TRI were similar in *Col4a1* HANAC mutant mice and controls (4 animals/group and per muscle). **D:** Histologic analysis of muscles in $Col4a1^{+/+}$, $Col4a1^{+/G498V}$, and $Col4a1^{G498V/G498V}$ female mice at 6 months of age. Cryosections of TRI were stained with hematoxylin and eosin (HE). Centronucleated fibers were observed frequently in $Col4a1^{+/G498V}$ and $Col4a1^{G498V/G498V}$ animals, but barely detectable in $Col4a1^{+/+}$. Inflammatory infiltrates were observed focally around muscle arterioles, mainly in $Col4a1^{G498V/G498V}$ mice. Sirius red (SR) staining of TRI muscle cryosections showed an abnormal accumulation of interstitial collagens in endomysium of *Col4a1* HANAC muscles. Quadriceps (QUAD) sections stained with Masson trichrome (MT) showing extravascular leakage of red blood cells in endomysium in both heterozygous and homozygous animals. Macroscopic intramuscular hemorrhages (**white arrows**) also occasionally were observed at the time of sacrifice in heterozygous and more frequently in homozygous mutants (photographs TRI). **E:** Quantification of centronucleated fibers in TA and TRI (3 animals/group and per muscle). **F:** Quantification of TA, TRI, and QUAD fibrosis performed on cryosections stained with SR (3 animals/group, 6 muscles/animal). Data are expressed as means ± SD (**B**, **C**, **E** and **F**). $*P < 0.05$, $**P < 0.01$, and $***P < 0.001$. **D:** Scale bars: 50 µm (**D, top 4 rows**); 0.5 mm (**D, bottom row**).

(Figure 1F). The extent of fibrosis was significantly greater in TA and QUAD muscles of homozygous mutants than of heterozygous mice (Figure 1F). Focal inflammatory infiltrates were present in homozygous mutants, mainly around arterioles (Figure 1D). In addition to dystrophic changes, macroscopic intramuscular hemorrhages were seen occasionally in mutant animals of both genotypes, with Masson trichrome staining showing focal areas of extravascular leakage of red blood cells in endomysium (Figure 1D).

Altogether, these observations indicated that *Col4a1* HANAC mutant mice develop a muscular dystrophy characterized by a muscle mass decrease resulting from fiber atrophy, an increased number of centronucleated fibers, fibrosis, focal perivascular inflammation, intramuscular hemorrhages, and mild muscle regeneration. Homozygous mutant animals were affected more severely.

Remodeling of the Skeletal Muscle ECM

We further analyzed the skeletal muscle expression of ECM proteins by immunostaining (Figure 2). Several ECM components, including collagen I, collagen VI, perlecan, and fibronectin, accumulated in endomysium of *Col4a1* mutant muscles (Figure 2A). An increased labeling of endothelial cells and sarcolemma with anti-integrin β1 antibodies also was observed (Figure 2A and Supplemental Figure S2). Expression of dystrophin was preserved in sarcolemma of mutant muscles (Figure 2A) and incubation of unfixed TRI cryosections with mouse IgG did not show abnormal labeling of the myofiber sarcoplasm, indicating the preserved integrity of the sarcolemma (Supplemental Figure S3). Collagen IV analysis showed a reduction of α1(IV) and α2(IV) chain expression in muscle BM, mostly in homozygous, but also in heterozygous, mutant animals

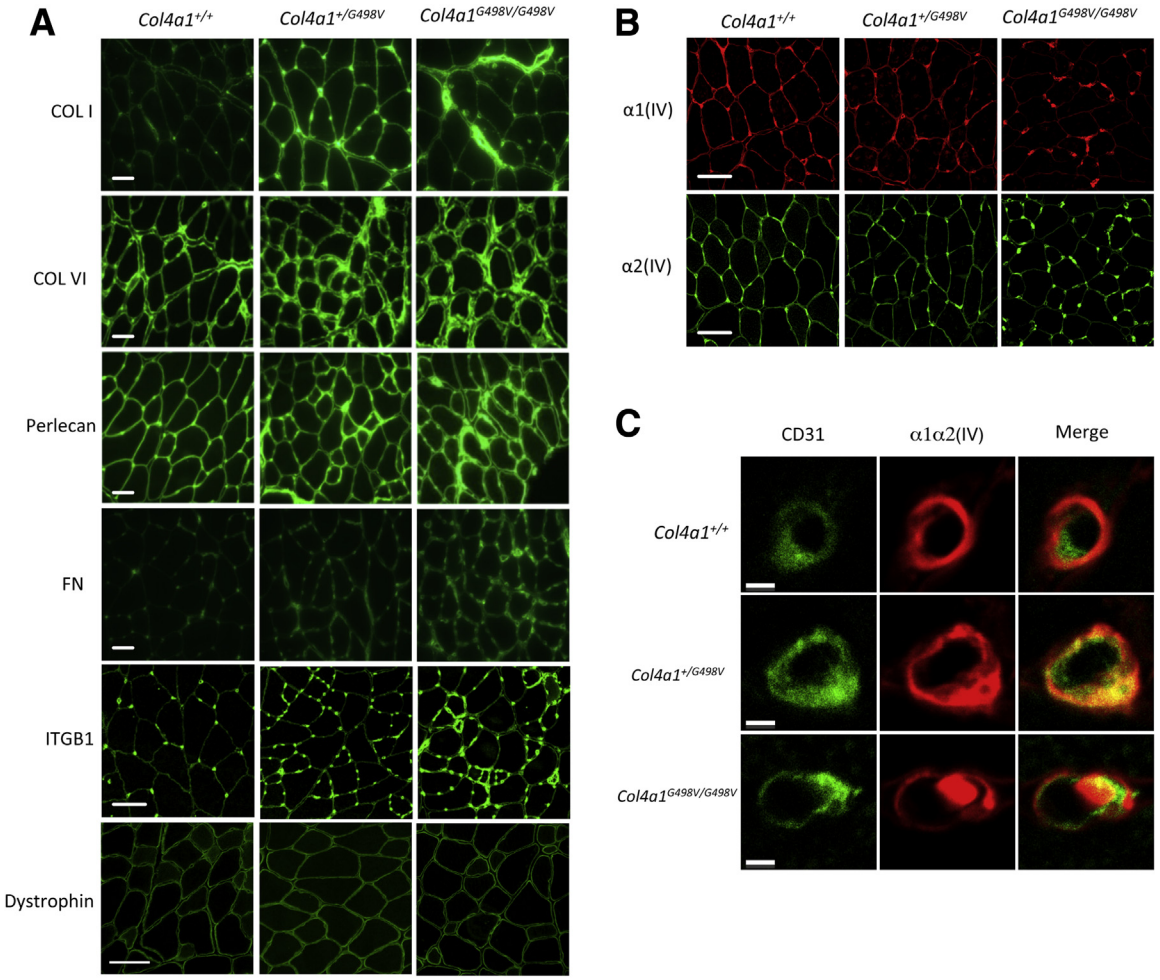

Figure 2 ECM remodeling, integrin β1, and dystrophin expression in HANAC muscles. **A:** Collagen I (COLI), collagen VI (COLVI), perlecan, and fibronectin (FN) accumulated abnormally in the *Col4a1* mutant muscle endomysium and basement membrane (BM) (TA muscle). Sarcolemmal and endothelial cell expression of the integrin β1 subunit was increased in *Col4a1*$^{+/G498V}$ and *Col4a1*$^{G498V/G498V}$ animals (TA muscle). Expression of dystrophin was comparable between genotypes. **B:** Immunolabeling with monoclonal anti—collagen IV α1 antibody (H11), and anti—collagen IV α2 antibody (H22), showing a reduction of collagen IV expression in the muscle BM, and an intense labeling of the endothelial cells (TA muscle). **C:** Co-immunostaining using polyclonal anti-α1α2(IV) (green) and anti-CD31 (red) antibodies, showing an increased labeling of collagen IV in CD31-positive endothelial cells of capillaries, that was more intense in *Col4a1*$^{G498V/G498V}$ animals (TRI muscle). Scale bars: 50 μm (**A** and **B**); 2 μm (**C**). ITGB1, integrin β1.

(Figure 2B), indicating that the *Col4a1 p.G498V* mutation partially impaired the α1α1α2(IV) trimer formation and/or its secretion. Concomitantly, we observed an intense labeling of collagen IV within CD31-positive cells, suggesting intracellular accumulation of both α1(IV) and α2(IV) chains in endothelial cells of the muscle capillaries of the mutant mice, whereas myofibers did not show increased intracellular collagen IV staining (Figure 2C). Ultrastructural analysis also disclosed ECM defects in TA and extensor digitorum longus muscles, with endomysium thickening caused by abnormal accumulation of interstitial fibrosis. Muscle basal lamina in mutant animals was irregular, focally duplicated, and vanishing with a lower electron density, and adjacent sarcolemma showed more invaginations (Figure 3, A–C). The ultrastructural aspect of myofibers and the morphology of the sarcoplasmic reticulum and mitochondria remained normal in mutant muscles (Figure 3, D–I).

Morphologic Endothelial Cell Alterations in HANAC Muscle

We specifically focused our analysis on endothelial cells because most of the clinical symptoms observed in *Col4a1*-associated diseases are related to microvascular defects. By electron microscopy, we observed abnormal enlargement of endoplasmic reticulum (ER) cisternae within endothelial cells in mutant muscles (Figure 3, G–I). No ER dilations were observed in endomysial cells other than endothelial cells. These results, together with our observation of α1(IV) and α2(IV) chain intracellular retention, suggested that mutant misfolded α1α1α2(IV) trimers most likely accumulated in ER in endothelial cells. In addition, a 2.2- and 3.8-fold increase in the number of CD31-positive endothelial cells was observed in muscle endomysium of heterozygous and homozygous mice, respectively ($P < 0.001$) (Figure 4).

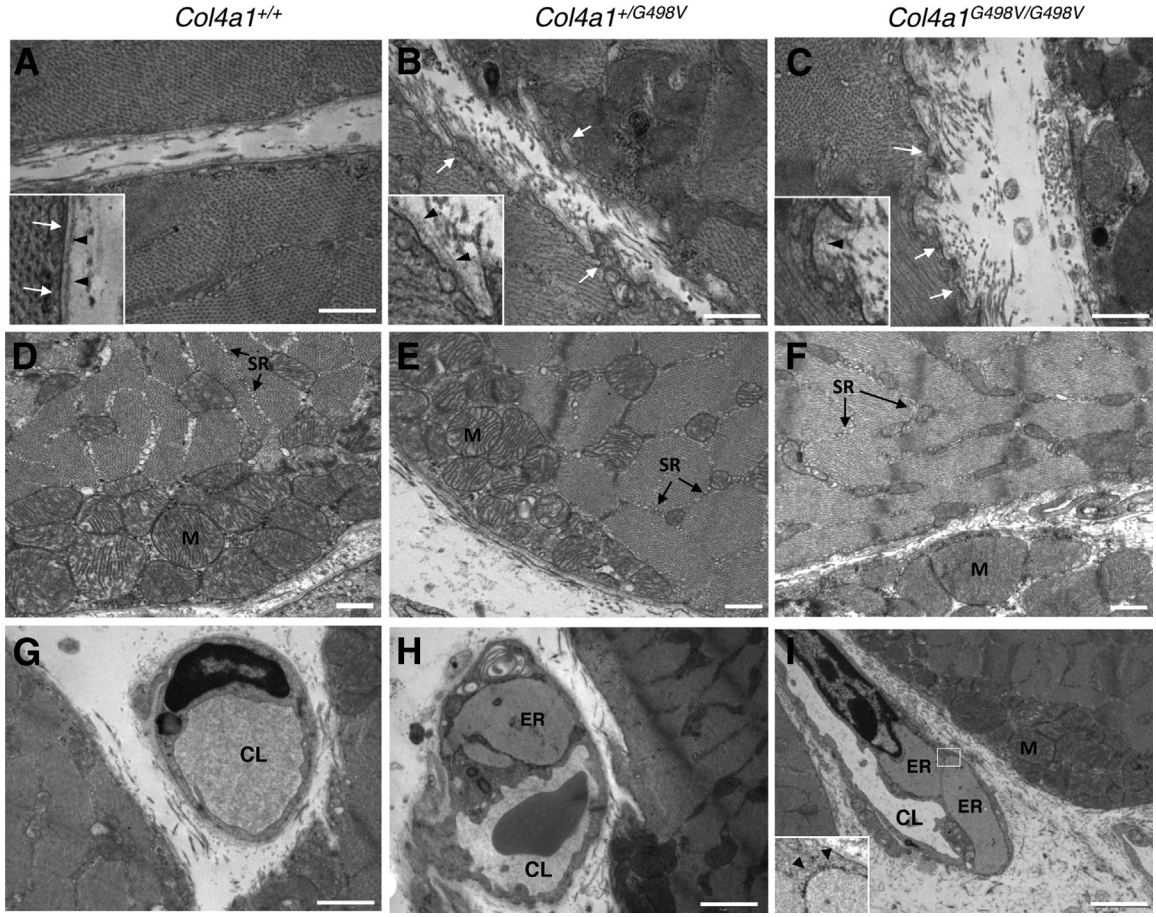

Figure 3 Ultrastructural defects in *Col4a1* HANAC muscles. Electron microscopy analysis of extensor digitorum longus muscles. **A–C:** Abnormal accumulation of fibrillar collagens in endomysium, with irregular aspect of sarcolemma (**white arrows**) and reduced electron density of the basal lamina (**black arrowheads**) in both heterozygous and homozygous *Col4a1* HANAC mutant muscles compared with controls. **Insets** show high magnifications centred on the sarcolemma and the muscle basal lamina. **D–F:** Ultrastructural aspects of myofibers showing normal sarcoplasmic reticulum (**arrows**) and normal structure of mitochondria in heterozygous and homozygous muscles. **G–I:** Large dilations of endoplasmic reticulum in endothelial cells of the muscle capillaries in heterozygous (**H**) and homozygous (**I**) *Col4a1* HANAC mutant mice compared to wild type mice (**G**). **Inset** in **I** shows enlarged ER cisternae lined by ribosomes in homozygous *Col4a1* HANAC mutant mice from the **boxed area** of the main image at high magnification. Scale bars: 0.5 μm (**A–F**); 2 μm (**G–I**). Original magnification: ×50,000 (**insets**). CL, capillary lumen; ER, endoplasmic reticulum; M, mitochondria; SR, sarcoplasmic reticulum.

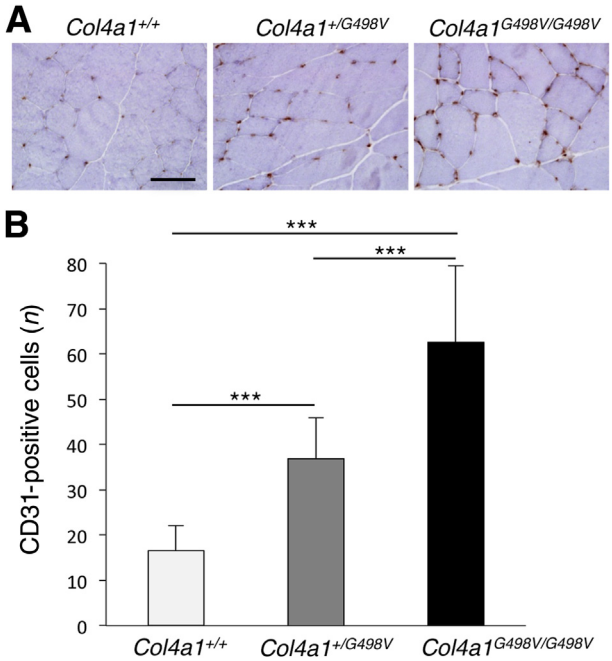

Figure 4 Increased CD31-positive endothelial cells in muscle in *Col4a1* HANAC mutant mice. **A:** Immunostaining of quadriceps muscles of *Col4a1*$^{+/+}$, *Col4a1*$^{+/G498V}$, and *Col4a1*$^{G498V/G498V}$ mice using an anti-CD31 antibody. **B:** Quantification of CD31-positive endothelial cells in quadriceps muscle. $n = 3$ animals of each genotype. Data are expressed as means ± SD. ***$P < 0.001$. Scale bar = 50 μm.

Induction of Endothelial Cell ER Stress and Apoptosis in HANAC Muscle

We further investigated whether ultrastructural ER morphologic changes and intracellular α1α2(IV) accumulation in endothelial cells of muscle were associated with induction of ER stress. Immunofluorescence staining of the binding immunoglobulin protein, protein disulfide isomerase, and heat shock protein 47, an ER resident chaperone, showed overexpression specifically in CD31-positive endothelial cells in *Col4a1* mutant muscles (Figure 5, A–C). We detected an eightfold increase of X-box–binding protein 1 spliced mRNA specifically in mutant animals, without mRNA level increase of the X-box–binding protein 1 unspliced form (Figure 5D). Western blot experiments also disclosed an increased expression of heat shock protein 47 and key ER stress proteins expression, including BiP; calnexin; protein disulfide isomerase; and C/EBP-enhancer–binding homologous protein in muscle protein extracts of mutant mice (Figure 5E). Because C/EBP-enhancer–binding homologous protein is a pro-apoptotic transcription factor specifically related to the unfolded protein response (UPR), we investigated cell apoptosis in muscles. An excess of terminal deoxynucleotidyl transferase-mediated dUTP nick-end labeling–positive apoptotic nuclei was detected in the endomysium of *Col4a1*$^{G498V/G498V}$ muscles, suggesting that apoptosis might affect endothelial cells specifically (Figure 6, A and B). In addition, caspase-12 and caspase-3 activities were enhanced in muscle protein extracts of mutant muscles (Figure 6, C and D). Altogether, these data strongly suggested that ER accumulation of the misfolded α1α1α2(IV) mutant trimers induced UPR, leading to ER stress in muscle endothelial cells, and resulted in a dramatic enhancement of apoptosis in this cell population.

HANAC Myopathy Is Associated with a Decrease of Maximal Force and an Increase of Serum Creatine Kinase Level

To determine whether morphologic muscle defects were associated with an alteration of functional performance, *in situ* muscle forces were evaluated in 6-month-old wild-type and *Col4a1*$^{+/G498V}$ mice of both sexes. The absolute maximal force and the specific maximal force of TA muscles were reduced significantly by 25.5% and 14.4%, respectively, compared with wild-type animals (Figure 7, A and B). At this age, we also observed a muscle weight decrease of −13.3% ($P = 0.015$) in heterozygous animals.

In addition, we observed a significant mild increase of serum CK level in heterozygous and homozygous 3-month-old mutant mice at rest, as compared with controls, however, with variability among animals within genotype groups (Figure 7C).

Discussion

We recently established the first experimental model of the HANAC syndrome, the *Col4a1*–G498V mutant mice, and we showed that these mutant mice constitute a relevant model for the analysis of the pathophysiology of the renal defects in HANAC syndrome.[21] In the present study, we provide new insights into the mechanisms of the skeletal muscle involvement, which is a major feature of this syndrome. Striated muscle BM contains from the α1α2(IV) collagen IV network. Morphologic alterations of myofibers and muscular functional defects were observed in *Drosophila Col4a1* mutant series,[23] as well as an increase of serum CK and an increase of centronucleated fibers in *Col4a1*$^{+/\Delta ex41}$ N-ethyl N-nitrosourea mutant mice.[24] We now show that *Col4a1*^{G498V} animals have morphologic defects that share characteristics with inherited muscular dystrophies, which are characterized by a disruption of the sarcolemma–ECM connection related to intracellular, transmembrane, or extracellular protein mutations.[25] At the ultrastructural level, the electron density of the muscle basal lamina of *Col4a1*^{G498V} animals was decreased, while the adjacent sarcolemma showed focal irregular aspects. In addition to alterations of intrinsic mechanical properties of the mutant BM collagen IV network, defective interactions between Col4a1^{G498V} mutant protein and other BM components or relevant cell adhesion molecules may account for pathologic defects in HANAC muscles. Indeed, collagen IV interacts with

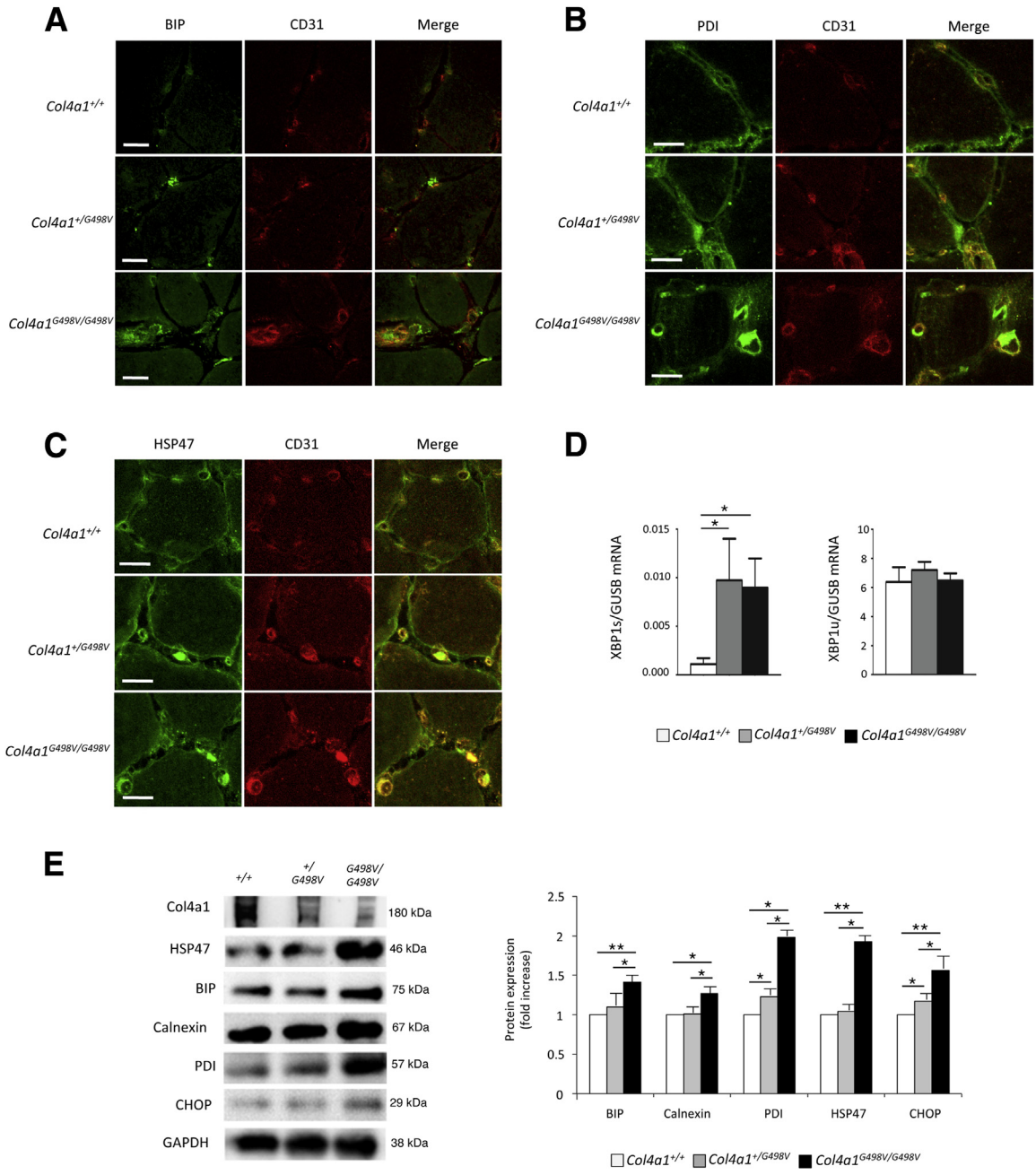

Figure 5 Induction of endoplasmic reticulum stress in endothelial cells in *Col4a1* HANAC mutant mice. **A**–**C:** Cryosections of quadriceps (QUAD) were co-immunostained with anti-CD31 (red) and anti–binding immunoglobulin protein (BIP) (**A**), protein disulfide isomerase (PDI) (**B**), and heat shock protein (HSP) 47 (**C**) (green) antibodies, respectively. Confocal microscopy analysis showed intense expression of ER stress proteins and HSP47 in CD31-positive endothelial cells. **D:** Quantitative PCR analysis of mRNA expression level of X-box–binding protein 1 spliced (XBP1s) (**left panel**) and X-box-binding protein 1 unspliced (XBP1u) (**right panel**), normalized with β-glucuronidase (GUSB), showed a significant increase of the XBP1s in both heterozygous and homozygous animals. Experiments were performed in triplicate. **E:** Western blot analysis of protein extracts from QUAD muscle and quantification. Expression of the α1 and α2 chains of collagen IV was strongly reduced in *Col4a1* mutant muscles, whereas the HSP47 collagen-specific chaperone was increased. ER stress proteins including BIP; calnexin; PDI; and C/EBP homologous protein (CHOP) proteins were increased significantly in $Col4a1^{G498V/G498V}$ animals, with PDI and CHOP also increased in $Col4a1^{+/G498V}$ muscles (3 animals/group). $n = 3$ animals per group (**E**); $n = 3$ $Col4a1^{+/+}$ (**D**); $n = 6$ $Col4a1^{+/G498V}$ (**D**); $n = 8$ $Col4a1^{G498V/G498V}$ (**D**). $^{*}P < 0.05$, $^{**}P < 0.01$. Scale bars = 20 μm. GAPDH, glyceraldehyde-3-phosphate dehydrogenase; GUSB, beta glucuronidase.

collagen VI, whose genes mutations are responsible for Ullrich congenital muscular dystrophy, Bethlem myopathy, and myosclerosis.[26] Moreover, defective interaction between HANAC mutant α1α1α2(IV) heterotrimer and the α7β1 integrin expressed in myofibers can be suspected because among *COL4A1*-related diseases, muscle symptoms are a constant feature of HANAC patients who all bear a *COL4A1* mutation specifically located in the G498–G525 region of the protein, which contains several integrin-binding sites. This hypothesis is supported by the

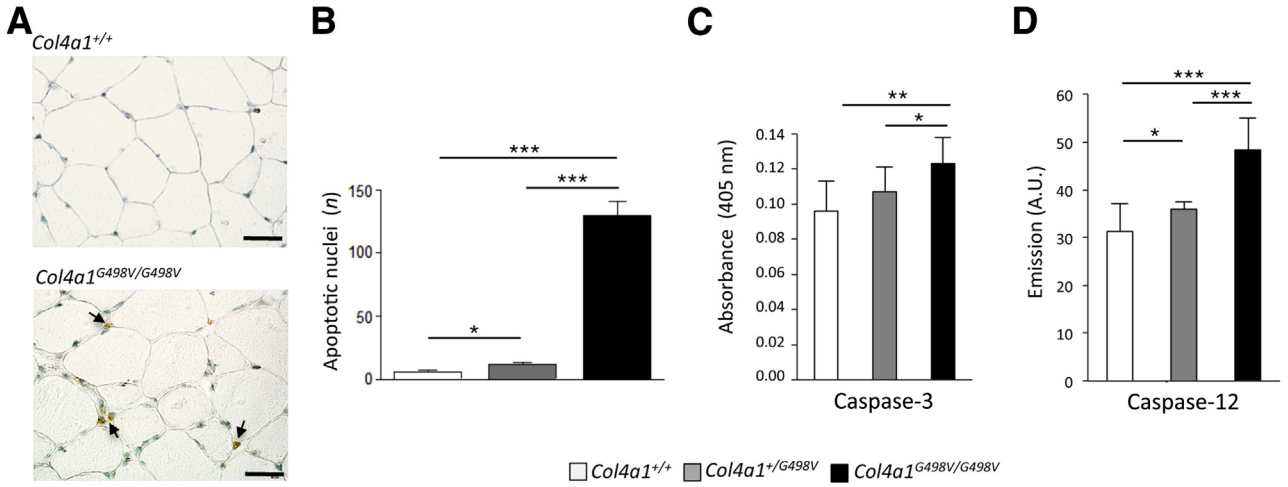

Figure 6 Increased apoptosis in *Col4a1* HANAC mutant muscle. **A:** Terminal deoxynucleotidyl transferase-mediated dUTP nick-end labeling (TUNEL)-labeled sections of triceps (TRI) of 6-month-old female mice counterstained with methyl green. TUNEL-positive nuclei, labeled in brown (**arrows**), were present in excess in the endomysium of *Col4a1*$^{G498V/G498V}$ muscle. **B:** Quantification of apoptotic nuclei in TRI muscle of 6-month-old *Col4a1*$^{+/+}$, *Col4a1*$^{+/G498V}$, and *Col4a1*$^{G498V/G498V}$ female mice (3 animals/group, 3 whole transverse muscle sections/animals). **C:** Quantification of caspase-3 activity determined in duplicate in TRI protein extracts (4 animals/group). **D:** Quantification of caspase-12 activity determined in duplicate in TRI protein extracts (4 animals/group). Data are expressed as means ± SD. $*P < 0.05$, $**P < 0.01$, $***P < 0.001$. Scale bars = 50 μm. A.U., arbitrary unit.

increased β1 integrin expression in the HANAC skeletal muscle, which may compensate defective collagen IV/myofiber interaction. At variance with *Col4a1*$^{\Delta ex41/\Delta ex41}$ mice that lack extracellular α1α1α2(IV) trimers, the *Col4a1 p.G498V* mutation did not completely abolish the assembly and secretion of the mutant protein in the muscle as well as in the kidney,[21] which may explain the less severe phenotype of HANAC *Col4a1*−G498V mutant mice. *In vitro* observations also showed that the degree of mutant α1(IV) intracellular retention was influenced by the location of the mutations, those located at the C-terminal part of the protein were associated with higher intracellular accumulation and more severe organ defects.[27,28]

A mild degenerative/regenerative process was observed in *Col4a1*−G498V mutant muscles, with a significant increase of centronucleated fibers, and eMHC-positive cells in homozygous animals. The lack of increase in eMHC-positive fibers in heterozygous muscles at 6 months may be explained by the transient expression of eMHC in regenerating fibers.

Because myofiber defects remain moderate (preserved integrity of sarcolemma and organelles, and low increase of CK levels), muscle regeneration in our model may have resulted from fiber necrosis occurring at an earlier age, or could be the consequence of nondystrophic myopathic changes, notably owing to vascular alterations. Indeed, the dystrophic phenotype of HANAC muscle was associated with severe endothelial cell alterations, which represent a striking and original characteristic of HANAC myopathy and may contribute to muscle injury, together with an ECM-sarcolemma disconnection. Mutant α1α1α2 (IV) trimers accumulate within the ER of endothelial cells, leading to marked ER cisternae dilation and UPR activation. Both caspase-3 and caspase-12 activities were enhanced in *Col4a1*−G498V mutant mice, and homozygous mutant muscles showed a dramatic level of apoptosis that spared

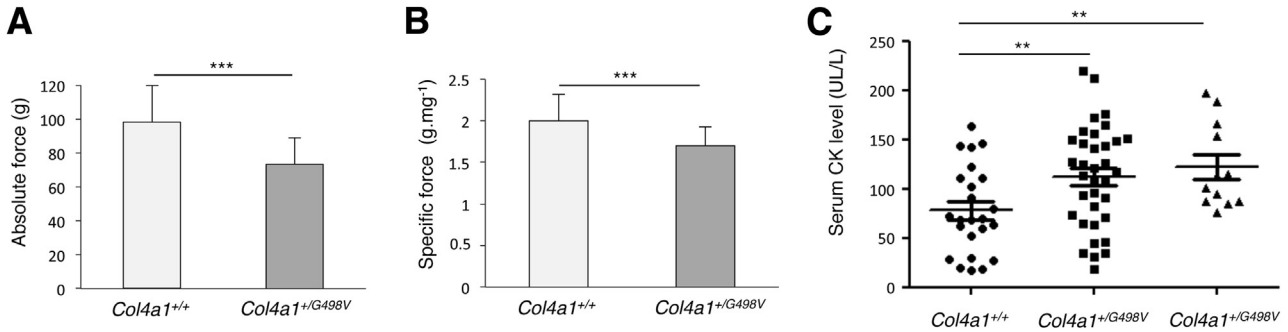

Figure 7 Functional muscular alterations and serum creatine kinase (CK) increase in *Col4a1* mutant mice. **A** and **B:** Contractile properties of the tibialis anterior muscle analyzed in 6-month-old *Col4a1*$^{+/+}$ and *Col4a1*$^{+/G498V}$ mice (5 females and 5 males in each genotype group) showed a decrease of the absolute maximal force (**A**) and of the specific maximal force defined as the absolute maximal force related to muscle weight (**B**). **C:** Serum creatine kinase levels in 3-month-old animals. Data are expressed as means ± SD. $n = 24$ *Col4a1*$^{+/+}$; $n = 35$ *Col4a1*$^{+/G498V}$; $n = 12$ *Col4a1*$^{G498V/G498V}$. $**P < 0.01$, $***P < 0.001$.

myofibers as a consequence of cytotoxic effects of UPR in endothelial cells. ER stress induction was shown previously in lens epithelium of *Col4a1*$^{+/\Delta ex41}$ mice, and transcriptional induction of binding immunoglobulin protein mRNA was reported in aorta of *Col4a1* Raw mice.[29,30] Jeanne et al[28] recently reported abnormal intracellular accumulation of the α1α2(IV) chains in endothelial cells of retinal arteries in *Col4a1*$^{+/\Delta ex41}$ mice. At variance with HANAC mice, *Col4a1*$^{\Delta ex41}$ mice showed a severe cerebrovascular brain phenotype with embryonic lethality of homozygous animals and a high rate of mortality of heterozygous mice at 1 month, mostly related to intracerebral hemorrhages. Treatment with the chemical chaperone sodium 4-phenylbutyrate reduced intracerebral hemorrhage severity in *Col4a1*$^{+/\Delta ex41}$ animals through enhanced collagen IV BM secretion and decreased cellular accumulation.[28] Such therapeutic intervention also could be effective in improving, at least in part, the muscle phenotype in HANAC syndrome.

Clinical and experimental data have pointed out the potential primary or secondary role of muscle vasculature defects in either inherited or acquired myopathies. In *mdx* mice and patients with Duchenne or Becker muscular dystrophy, muscle ischemia is suspected to accelerate injury of muscle fibers caused by defective sarcolemmal neuronal nitrite oxide synthase and alterations in nitrite oxide production.[31] Strategies that boost nitrite oxide signaling improved the dystrophic phenotype of *mdx* mice, and restored normal muscle blood flow in patients with Becker myopathy.[32,33] Further studies are required to assess the consequences of the endothelial cell defects on tissue hypoxia and inflammation, which might contribute to the endothelial cell proliferation observed in *Col4a1* HANAC mutant muscles, and, more generally, may provide insight into the mechanisms of cramps.

The phenotype of *Col4a1*−G498V homozygous mice is more severe than the one observed in heterozygous animals, suggesting that haploinsufficiency may impact the phenotype severely, in addition to the dominant-negative effect of the col4a1 mutant protein that induced ER retention and UPR activation. However, morphologic muscle anomalies, functional alterations, and ER defects in endothelial cells also have been observed in heterozygous mutant animals. Interestingly, in HANAC patients, muscle cramps are enhanced on exposition to cold temperature. This trigger event is similar to the one responsible for Raynaud phenomena, suggesting altered microvascular reactivity also in skeletal muscle. A biopsy specimen of quadriceps in one patient with HANAC did not show an ultrastructural fiber alteration or an endothelial cell defect, although histologic signs of myopathy were characterized in one patient with a *COL4A1*-pathogenic variant.[12] Results arising from murine preclinical models must usually be translated carefully into the human pathophysiology because several additional factors, including genetic background and environmental modifiers, may influence phenotypic expression of the monogenic trait.

In conclusion, this study on the muscle phenotype of *Col4a1* HANAC mutant mice shows the important role of the collagen IV network in maintaining the integrity of the ECM-sarcolemmal connection in skeletal muscle. It also suggests the potential contributing role of local microvascular defects in the genesis of the muscle phenotype, through *in vivo* UPR induction related to abnormal accumulation of the mutant protein in endothelial cells. These data open up new perspectives in the field of muscular dystrophies, which may help to delineate new therapeutic interventions that specifically target the muscular microvascular compartment.

Acknowledgments

We thank Chantal Jouanneau (INSERM UMR 1155, Paris, France), Sandra Onifarasoaniaina (INSERM UMR 1155, Paris, France), and Daniel Stockholm (Imaging-Cytometry of Généthon, Evry, France) for their technical assistance, and Jeanne Lainé (UMRS974, Institute of Myology, Paris, France) for helpful discussions with electron microscopy analysis.

Supplemental Data

Supplemental material for this article can be found at *http://dx.doi.org/10.1016/j.ajpath.2016.10.020*.

References

1. Kalluri R: Basement membranes: structure, assembly and role in tumour angiogenesis. Nat Rev Cancer 2003, 3:422−433
2. Khoshnoodi J, Pedchenko V, Hudson BG: Mammalian collagen IV. Microsc Res Tech 2008, 71:357−370
3. Lampe AK, Bushby KM: Collagen VI related muscle disorders. J Med Genet 2005, 42:673−685
4. Helbling-Leclerc A, Zhang X, Topaloglu H, Cruaud C, Tesson F, Weissenbach J, Tomé FM, Schwartz K, Fardeau M, Tryggvason K, Guicheney P: Mutations in the laminin alpha 2-chain gene (LAMA2) cause merosin-deficient congenital muscular dystrophy. Nat Genet 1995, 11:216−218
5. Mayer U, Saher G, Fässler R, Bornemann A, Echtermeyer F, von der Mark H, Miosge N, Pöschl E, von der Mark K: Absence of integrin alpha 7 causes a novel form of muscular dystrophy. Nat Genet 1997, 17:318−323
6. Godfrey C, Foley AR, Clement E, Muntoni F: Dystroglycanopathies: coming into focus. Curr Opin Genet Dev 2011, 21:278−285
7. Gould DB, Phalan FC, Breedveld GJ, van Mil SE, Smith RS, Schimenti JC, Aguglia U, van der Knaap MS, Heutink P, John SW: Mutations in Col4a1 cause perinatal cerebral hemorrhage and porencephaly. Science 2005, 308:1167−1171
8. Breedveld G, de Coo IF, Lequin MH, Arts WF, Heutink P, Gould DB, John SW, Oostra B, Mancini GM: Novel mutations in three families confirm a major role of COL4A1 in hereditary porencephaly. J Med Genet 2006, 43:490−495
9. Gould DB, Phalan FC, van Mil SE, Sundberg JP, Vahedi K, Massin P, Bousser MG, Heutink P, Miner JH, Tournier-Lasserve E, John SW:

Role of COL4A1 in small-vessel disease and hemorrhagic stroke. N Engl J Med 2006, 354:1489–1496
10. Lanfranconi S, Markus HS: COL4A1 mutations as a monogenic cause of cerebral small vessel disease: a systematic review. Stroke 2010, 41: e513–e518
11. Coupry I, Sibon I, Mortemousque B, Rouanet F, Mine M, Goizet C: Ophthalmological features associated with COL4A1 mutations. Arch Ophthalmol 2010, 128:483–489
12. Yoneda Y, Haginoya K, Kato M, Osaka H, Yokochi K, Arai H, Kakita A, Yamamoto T, Otsuki Y, Shimizu S, Wada T, Koyama N, Mino Y, Kondo N, Takahashi S, Hirabayashi S, Takanashi J, Okumura A, Kumagai T, Hirai S, Nabetani M, Saitoh S, Hattori A, Yamasaki M, Kumakura A, Sugo Y, Nishiyama K, Miyatake S, Tsurusaki Y, Doi H, Miyake N, Matsumoto N, Saitsu H: Phenotypic spectrum of COL4A1 mutations: porencephaly to schizencephaly. Ann Neurol 2013, 73:48–57
13. Plaisier E, Gribouval O, Alamowitch S, Mougenot B, Prost C, Verpont MC, Marro B, Desmettre T, Cohen SY, Roullet E, Dracon M, Fardeau M, Van Agtmael T, Kerjaschki D, Antignac C, Ronco P: COL4A1 mutations and hereditary angiopathy, nephropathy, aneurysms, and muscle cramps. N Engl J Med 2007, 357:2687–2695
14. Alamowitch S, Plaisier E, Favrole P, Prost C, Chen Z, Van Agtmael T, Marro B, Ronco P: Cerebrovascular disease related to COL4A1 mutations in HANAC syndrome. Neurology 2009, 73:1873–1882
15. Plaisier E, Chen Z, Gekeler F, Benhassine S, Dahan K, Marro B, Alamowitch S, Paques M, Ronco P: Novel COL4A1 mutations associated with HANAC syndrome: a role for the triple helical CB3(IV) domain. Am J Med Genet A 2010, 152A:2550–2555
16. Vandenberg P, Kern A, Ries A, Lickenbill-Edds L, Mann K, Kühn K: Characterization of a type IV collagen major cell binding site with affinity to the alpha 1 beta 1 and the alpha 2 beta 1 integrins. J Cell Biol 1991, 113:1475–1483
17. Knight CG, Morton LF, Peachey AR, Tuckwell DS, Farndale RW, Barnes MJ: The collagen-binding A-domains of integrins alpha(1) beta(1) and alpha(2)beta(1) recognize the same specific amino acid sequence, GFOGER, in native (triple-helical) collagens. J Biol Chem 2000, 275:35–40
18. Renner C, Sacca B, Moroder L: Synthetic heterotrimeric collagen peptides as mimics of cell adhesion sites of the basement membrane. Biopolymers 2004, 76:34–47
19. Van Agtmael T, Bailey MA, Schlötzer-Schrehardt U, Craigie E, Jackson IJ, Brownstein DG, Megson IL, Mullins JJ: Col4a1 mutation in mice causes defects in vascular function and low blood pressure associated with reduced red blood cell volume. Hum Mol Genet 2010, 19:1119–1128
20. Favor J, Gloeckner CJ, Janik D, Klempt M, Neuhäuser-Klaus A, Pretsch W, Schmahl W, Quintanilla-Fend L: Type IV procollagen missense mutations associated with defects of the eye, vascular stability, the brain, kidney function and embryonic or postnatal viability in the mouse, Mus musculus: an extension of the Col4a1 allelic series and the identification of the first two Col4a2 mutant alleles. Genetics 2007, 175:725–736
21. Chen Z, Migeon T, Verpont MC, Zaidan M, Sado Y, Kerjaschki D, Ronco P, Plaisier E: HANAC syndrome Col4a1 mutation causes neonate glomerular hyperpermeability and adult glomerulocystic kidney disease. J Am Soc Nephrol 2016, 27:1042–1054
22. Ferry A, Joanne P, Hadj-Said W, Vignaud A, Lilienbaum A, Hourdé C, Medja F, Noirez P, Charbonnier F, Chatonnet A, Chevessier F, Nicole S, Agbulut O, Butler-Browne G: Advances in the understanding of skeletal muscle weakness in murine models of diseases affecting nerve-evoked muscle activity, motor neurons, synapses and myofibers. Neuromuscul Disord 2014, 24: 960–972
23. Kelemen-Valkony I, Kiss M, Csiha J, Kiss A, Bircher U, Szidonya J, Maróy P, Juhász G, Komonyi O, Csiszár K, Mink M: Drosophila basement membrane collagen col4a1 mutations cause severe myopathy. Matrix Biol 2012, 31:29–37
24. Labelle-Dumais C, Dilworth DJ, Harrington EP, de Leau M, Lyons D, Kabaeva Z, Manzini MC, Dobyns WB, Walsh CA, Michele DE, Gould DB: COL4A1 mutations cause ocular dysgenesis, neuronal localization defects, and myopathy in mice and Walker-Warburg syndrome in humans. PLoS Genet 2011, 7:e1002062
25. Rahimov F, Kunkel LM: The cell biology of disease: cellular and molecular mechanisms underlying muscular dystrophy. J Cell Biol 2013, 201:499–510
26. Kuo HJ, Maslen CL, Keene DR, Glanville RW: Type VI collagen anchors endothelial basement membranes by interacting with type IV collagen. J Biol Chem 1997, 272:26522–26559
27. Kuo DS, Labelle-Dumais C, Mao M, Jeanne M, Kauffman WB, Allen J, Favor J, Gould DB: Allelic heterogeneity contributes to variability in ocular dysgenesis, myopathy and brain malformations caused by Col4a1 and Col4a2 mutations. Hum Mol Genet 2014, 23: 1709–1722
28. Jeanne M, Jorgensen J, Gould DB: Molecular and genetic analyses of collagen type IV mutant mouse models of spontaneous intracerebral hemorrhage identify mechanisms for stroke prevention. Circulation 2015, 131:1555–1565
29. Van Agtmael T, Schlötzer-Schrehardt U, McKie L, Brownstein DG, Lee AW, Cross SH, Sado Y, Mullins JJ, Pöschl E, Jackson IJ: Dominant mutations of Col4a1 result in basement membrane defects which lead to anterior segment dysgenesis and glomerulopathy. Hum Mol Genet 2005, 14:3161–3168
30. Gould DB, Marchant JK, Savinova OV, Smith RS, John SW: Col4a1 mutation causes endoplasmic reticulum stress and genetically modifiable ocular dysgenesis. Hum Mol Genet 2007, 16:798–807
31. Sander M, Chavoshan B, Harris SA, Lannaccone ST, Stull JT, Thomas GD, Victor RG: Functional muscle ischemia in neuronal nitric oxide synthase-deficient skeletal muscle of children with Duchenne muscular dystrophy. Proc Natl Acad Sci U S A 2000, 97: 13818–13823
32. Adamo CM, Dai DF, Percival JM, Minami E, Willis MS, Patrucco E, Froehner SC, Beavo JA: Sildenafil reverses cardiac dysfunction in the mdx mouse model of Duchenne muscular dystrophy. Proc Natl Acad Sci U S A 2010, 107:19079–19083
33. Martin EA, Barresi R, Byrne BJ, Tsimerinov EI, Scott BL, Walker AE, Gurudevan SV, Anene F, Elashoff RM, Thomas GD, Victor RG: Tadalafil alleviates muscle ischemia in patients with Becker muscular dystrophy. Sci Transl Med 2012, 4:162ra155